



**HAL**  
open science

# Nonlinear and Non-Gaussian Ensemble Assimilation of MOPITT CO

Benjamin Gaubert, Jeffrey Anderson, Michael Trudeau, Nadia Smith, Kathryn Mckain, Gabrielle Pétron, Kevin Raeder, Avelino Arellano, Claire Granier, Louisa Emmons, et al.

► **To cite this version:**

Benjamin Gaubert, Jeffrey Anderson, Michael Trudeau, Nadia Smith, Kathryn Mckain, et al.. Non-linear and Non-Gaussian Ensemble Assimilation of MOPITT CO. *Journal of Geophysical Research: Atmospheres*, 2024, 129 (12), 10.1029/2023JD040647 . hal-04793999

**HAL Id: hal-04793999**

**<https://hal.science/hal-04793999v1>**

Submitted on 9 Jan 2025

**HAL** is a multi-disciplinary open access archive for the deposit and dissemination of scientific research documents, whether they are published or not. The documents may come from teaching and research institutions in France or abroad, or from public or private research centers.

L'archive ouverte pluridisciplinaire **HAL**, est destinée au dépôt et à la diffusion de documents scientifiques de niveau recherche, publiés ou non, émanant des établissements d'enseignement et de recherche français ou étrangers, des laboratoires publics ou privés.

Copyright

# JGR Atmospheres

## RESEARCH ARTICLE

10.1029/2023JD040647

## Nonlinear and Non-Gaussian Ensemble Assimilation of MOPITT CO

### Key Points:

- A novel non Gaussian and nonlinear ensemble data assimilation (DA) framework is applied to MOPITT joint state/flux optimization
- The new method performs better than the Ensemble Adjustment Kalman Filter in comparison to independent observations
- MOPITT observations indicate that CAMS-GLOB-ANT\_v5.3 emission fluxes are underestimated across the mid-latitudes in May 2018

### Correspondence to:

B. Gaubert,  
gaubert@ucar.edu

### Citation:

Gaubert, B., Anderson, J. L., Trudeau, M., Smith, N., McKain, K., Pétron, G., et al. (2024). Nonlinear and non-Gaussian ensemble assimilation of MOPITT CO. *Journal of Geophysical Research: Atmospheres*, 129, e2023JD040647. <https://doi.org/10.1029/2023JD040647>

Received 20 DEC 2023

Accepted 4 JUN 2024

### Author Contributions:

**Conceptualization:** Benjamin Gaubert, Jeffrey L. Anderson

**Data curation:** Benjamin Gaubert, Michael Trudeau, Nadia Smith, Kathryn McKain, Gabrielle Pétron, Claire Granier, Ivan Ortega, James W. Hannigan, Wenfu Tang, Daniel Ziskin

**Formal analysis:** Benjamin Gaubert

**Funding acquisition:** Benjamin Gaubert

**Investigation:** Benjamin Gaubert

**Methodology:** Benjamin Gaubert

**Project administration:**

Benjamin Gaubert

**Resources:** Benjamin Gaubert

**Software:** Jeffrey L. Anderson, Michael Trudeau, Kevin Raeder, Louisa K. Emmons

**Supervision:** Benjamin Gaubert, Louisa K. Emmons, Helen M. Worden, David P. Edwards

**Validation:** Benjamin Gaubert











**Visualization:** Benjamin Gaubert

**Writing – original draft:**

Benjamin Gaubert, Jeffrey L. Anderson, Nadia Smith

**Writing – review & editing:**

Benjamin Gaubert, Michael Trudeau,

Benjamin Gaubert<sup>1</sup> , Jeffrey L. Anderson<sup>2</sup>, Michael Trudeau<sup>3,4</sup>, Nadia Smith<sup>5</sup>, Kathryn McKain<sup>4</sup> , Gabrielle Pétron<sup>3,4</sup>, Kevin Raeder<sup>2</sup> , Avelino F. Arellano Jr.<sup>6</sup>, Claire Granier<sup>3,7,8</sup> , Louisa K. Emmons<sup>1</sup> , Ivan Ortega<sup>1</sup> , James W. Hannigan<sup>1</sup> , Wenfu Tang<sup>1</sup> , Helen M. Worden<sup>1</sup> , Daniel Ziskin<sup>1</sup>, and David P. Edwards<sup>1</sup> 

<sup>1</sup>Atmospheric Chemistry Observations & Modeling Laboratory (ACOM), NSF National Center for Atmospheric Research (NSF NCAR), Boulder, CO, USA, <sup>2</sup>Computational and Information Systems Laboratory, NSF National Center for Atmospheric Research (NSF NCAR), Boulder, CO, USA, <sup>3</sup>Cooperative Institute for Research in Environmental Sciences, University of Colorado Boulder, Boulder, CO, USA, <sup>4</sup>Global Monitoring Laboratory, National Oceanic and Atmospheric Administration, Boulder, CO, USA, <sup>5</sup>Science and Technology Corporation, Columbia, MD, USA, <sup>6</sup>Department of Hydrology and Atmospheric Sciences, University of Arizona, Tucson, AZ, USA, <sup>7</sup>Chemical Sciences Laboratory, National Oceanic and Atmospheric Administration, Boulder, CO, USA, <sup>8</sup>Laboratoire d'Aérodynamique, Université de Toulouse, CNRS, UPS, Toulouse, France

**Abstract** Satellite retrievals of carbon monoxide (CO) are routinely assimilated in atmospheric chemistry models to improve air quality forecasts, produce reanalyses and to estimate emissions. This study applies the quantile-conserving ensemble filter framework, a novel assimilation algorithm that can deal with non-Gaussian and modestly nonlinear distributions. Instead of assuming normal distributions like the Ensemble Adjustments Kalman Filter (EAKF), we now apply a bounded normal rank histogram (BNRH) distribution for the prior. The goal is to efficiently estimate bounded quantities such as CO atmospheric mixing ratios and emission fluxes while maintaining the good performance achieved by the EAKF. We contrast assimilating meteorological and MOPITT (Measurement of Pollution in the Troposphere) observations for May 2018. We evaluate the results with the fourth deployment of the NASA Atmospheric Tomography Mission (ATom-4) airborne field campaign. We also compare simulations with CO tropospheric columns from the network for the detection of atmospheric composition change and surface in-situ observations from NOAA carbon cycle greenhouse gases. While the differences remain small, the BNRH approach clearly works better than the EAKF in comparison to all observation data sets.

**Plain Language Summary** The MOPITT instrument on the NASA/Terra satellite can detect carbon monoxide (CO) pollution in the lower and mid-tropospheric atmosphere but cannot accurately differentiate small changes in the altitude of pollution plumes. Such satellite observations are assimilated in numerical model predictions to improve the spatial and temporal distribution of CO in the atmosphere and to estimate emission fluxes. We present a novel method that does not require assumptions about the model and the observations, leading to a more efficient and accurate assimilation of the satellite observations.

## 1. Introduction

Capturing spatio-temporal variability of atmospheric constituents is important for both short-term air quality monitoring and multi-scale chemical weather forecasting (e.g., Brasseur & Kumar, 2021), as well as supporting chemistry-climate applications (e.g., Staniaszek et al., 2022). Carbon monoxide (CO) plays a central role in tropospheric chemistry. As the primary sink of the hydroxyl radical (OH), CO indirectly controls methane (CH<sub>4</sub>) lifetimes (Gaubert et al., 2017; Prather, 2007; Zhao et al., 2020), which may become increasingly important with the potential rise of hydrogen (H<sub>2</sub>) emissions (Bertagni et al., 2022).

Large scale episodic but ubiquitous wildfire sources of CO and other chemicals produce tropospheric ozone (O<sub>3</sub>) (Bourgeois et al., 2021; Jaffe & Wigder, 2012; Lin et al., 2017). Butler et al. (2018) estimated that CO contributes to around 10% of the global tropospheric O<sub>3</sub> burden. In combination with other data sets, satellite CO observations have proven useful in a number of different atmospheric applications, for example, to characterize urban environments (Silva et al., 2013; W. Tang et al., 2019; Wu et al., 2022), biogenic fluxes (Hudman et al., 2008; Parazoo

Kathryn McKain, Gabrielle Pétron,  
Kevin Raeder, Avelino F. Arellano Jr.,  
Claire Granier, Louisa K. Emmons,  
Ivan Ortega, Helen M. Worden

et al., 2021; Worden et al., 2019), ozone formation (Cheng et al., 2017, 2018), urban plume chemistry (Lama et al., 2022), wildfire emission trends (Buchholz et al., 2022) and chemistry (Juncosa Calahorrano et al., 2021) as well as long-range transport (Ceamanos et al., 2023).

The longest satellite record of CO column abundance retrievals is based on The Measurements of Pollution In The Troposphere (MOPITT) (Buchholz et al., 2021), and is used in reanalysis systems (Gaubert et al., 2017; Inness et al., 2019; Miyazaki et al., 2017) as well as inverse modeling to monitor emission and flux changes (Jiang et al., 2015; J. Liu et al., 2017; Zheng et al., 2019). Chemical DA efficiently integrates satellite observations to evaluate and improve models, estimate emissions, and issue chemical weather forecasts. As part of the Copernicus Atmosphere Monitoring Service or CAMS (Peuch et al., 2022), the European Center for Medium-Range Weather Forecasts (ECMWF) provides global air quality forecasts with MOPITT and Infrared Atmospheric Sounding Interferometer (IASI) CO DA (Inness et al., 2022) and will include operational real time assimilation of TROPOspheric Monitoring Instrument (TROPOMI). Satellite CO retrievals are considered to be the best observations to estimate fire emissions and are used to reduce uncertainties in the CO<sub>2</sub> budget (J. Liu et al., 2017; van der Velde et al., 2021; Naus et al., 2022; Zheng et al., 2023). Such CO observations also provide constraints on anthropogenic sources although discrepancies between bottom-up and top-down emissions remain in places such as China or western Africa (Elguindi et al., 2020). MOPITT inversions found that bottom-up CO emissions are underestimated in China, especially in the northern part of the country, with dominant contribution from the residential, the industrial and transportation sectors (Gaubert et al., 2020; Qu et al., 2022). CO inversions resulting from the assimilation of the S5P/TROPOMI observations indicated that industrial point sources were underestimated in bottom-up inventories between 2017 and 2020 in China (Tian et al., 2022). Inversions of satellite CO observations suggest a stronger seasonal cycle in CO emissions while the role of chemistry is also important and improving global chemistry models remains a challenge today (Gaubert et al., 2016, 2023; Kopacz et al., 2010; Shindell et al., 2006; Stein et al., 2014). Transport error, the hydroxyl radical OH, assimilation settings, as well as biases and vertical representativeness of satellite observations all contribute to error in inversions and complicate source attributions (Jiang et al., 2013; Müller et al., 2018; Z. Tang et al., 2022; Gaubert et al., 2023).

The goal of this study is to investigate the impact of the recently developed quantile-conserving ensemble filter framework (QCEFF) described in three publications (Anderson, 2022, 2023; Anderson et al., 2024). In past studies, we used of the Ensemble Adjustment Kalman Filter (EAKF) algorithm (Anderson, 2003) that assumes the prior model error and the observation error are normally distributed. For instance the CO chemistry is a coupled system that results in nonlinear sensitivity to initial conditions (Gaubert et al., 2016) and emissions, which impacts CH<sub>4</sub> (Gaubert et al., 2017). Here we introduce a non-Gaussian filter update that could outperform the EAKF in non-Gaussian cases while performing nearly as well as the EAKF otherwise. The analysis is performed using the bounded rank histogram filter and can represent arbitrary prior distributions for observed variables (Anderson, 2010, 2020). In addition to the nonlinear and non-Gaussian analysis updates, the localization, the inflation and the regression of unobserved variables are now perform in a transformed space that respects the appropriate bounds and can also better represent nonlinear relations between observed and unobserved state variables. We will refer to this analysis update as the bounded normal rank histogram (BNRH) assimilation algorithm (Anderson, 2023). This algorithm is designed specifically for positive-definite quantities such as CO atmospheric mixing ratios and emission fluxes.

We evaluate the different assimilation configuration results with MOPITT dry air columns (XCO), and three independent data sets that all cover a wide range of latitudes:

1. Global network of surface in-situ remote sites.
2. Dry-air tropospheric column-averaged mole fraction of CO from the Network for Detection of Atmospheric Composition Change (NDACC).
3. Aircraft in-situ profiles from the CO NASA airborne Atmospheric Tomography Mission (ATom)

This paper is organized as follows, we introduce the observations used for assimilation and evaluation in Section 2. The model and the assimilation algorithms are described in Section 3. Results of the assimilation experiments are compared to independent data sets in Section 4 and conclusions are presented in Section 5.

## 2. Observations

### 2.1. MOPITT V9J CO

We assimilate daytime observations of the most recent version 9 joint (V9J) MOPITT profile retrieval product, described and evaluated in Deeter et al. (2022). The version nine includes a bias correction algorithm introduced in V8 (Deeter et al., 2019) and shows comparable statistics with the evaluation data sets (Deeter et al., 2022). However, it includes an improved cloud detection algorithm that increases the number of retrievals and thus the spatial coverage (Deeter et al., 2021). The joint product shows a much larger vertical sensitivity by including CO absorption bands in both the near infrared (2.3  $\mu\text{m}$ ) and in the thermal infrared channels (4.7  $\mu\text{m}$ ) (Worden et al., 2010). Previous summertime assimilation of MOPITT V9J data showed improved modeled CO columns when compared to NDACC Fourier transform infrared (FTIR) tropospheric dry-air CO columns (Gaubert et al., 2023).

### 2.2. Network for Detection of Atmospheric Composition Change (NDACC)

We evaluate prior and optimized CO with the independent NDACC data set of ground-based Fourier transform infrared spectrometer (FTIR). The tropospheric mixing ratio of CO, weighted by air mass (wVMR), is obtained with ground-based FTIR measurements of cloud-free infrared spectra, with direct-sun observations. The station network includes remote and urban sites, in the southern hemisphere and at high latitudes of both hemispheres, but there is a lack of data in the tropics. For the considered period, there were 12 operating sites and 143 daytime average observations. For each observation, we apply the FTIR averaging kernels and a priori vertical profile to simulated vertical profiles to account for the FTIR altitude sensitivity. The impact of the tropopause is diminished by setting a maximum altitude lower than the height of the tropopause (Ortega et al., 2023).

### 2.3. NOAA Carbon Cycle Greenhouse Gases (CCGG)

We use the data from the CO GLOBALVIEWplus v2.0 ObsPack (Schuldt et al., 2021) provided by the NOAA Global Monitoring Laboratory. We selected the representative site of the surface in-situ network of flask sample CO measurements (Novelli, 2003; Novelli et al., 1991). The observations are average for the month of May 2018 and compared to the modeled monthly mean.

### 2.4. NASA Atmospheric Tomography Mission (ATom)

The fourth ATom deployment (ATom-4) occurred from 24 April to 21 May 2018 (Thompson et al., 2022). Here we use the flights number 4 to 12 from 1 May to 22 May 2018 and we separate the Atlantic and the Pacific at the meridian 70°W. The flight paths included vertical profiles reaching altitudes of up to 13 km. Figure 1 shows the DC-8 flight tracks and the resulting CO transects over the 2 different ocean basins. The CO mole fractions were measured in situ with a cavity ring down instrument (Picarro G2401 m). The south Pacific deployment constitutes flights 4 to 6 from 1 May to 7 May 2018. The Atlantic leg (flights 7 to 10) covered Antarctica to Greenland (Figures 1c and 1d), from 9 May to 18 May 2018. The northern parts of the Pacific transect were sampled with the last two flights. Since the campaign happened in the late boreal spring, the higher latitudes of the northern hemisphere show a large background CO, usually higher than 100 ppb. Conversely, the CO levels were lower than 80 ppb in the southern hemisphere and less than 50 ppb in the southern high latitudes.

## 3. Methods

### 3.1. Community Atmosphere Model With Chemistry (CAM-chem)

Simulations are conducted with the Community Atmosphere Model with Chemistry (CAM-chem), a configuration of the Community Earth System Model version 2.2 (CESM2.2), described in Danabasoglu et al. (2020). We use the standard chemistry configuration, which is the MOZART tropospheric and stratospheric chemistry TS1 (Emmons et al., 2020) and the modal aerosol model (X. Liu et al., 2016), including the updated Volatility Basis Set schemes for secondary organic aerosols (Tilmes et al., 2019). We only modify the nitric acid trihydrate particle number densities from 0.01 to  $10^{-5} \text{ cm}^{-3}$  to better represent stratospheric ozone (Bouarar et al., 2021; Wilka et al., 2021) and the heterogeneous aerosol uptake coefficient ( $\gamma$ ) of 0.1 for hydroperoxyl radical ( $\text{HO}_2$ ), with the reaction product being  $\text{H}_2\text{O}$  instead of  $\text{H}_2\text{O}_2$  following Gaubert et al. (2020). The model is run with 32 vertical layers on a  $0.95^\circ$  in latitude by  $1.25^\circ$  in longitude grid.

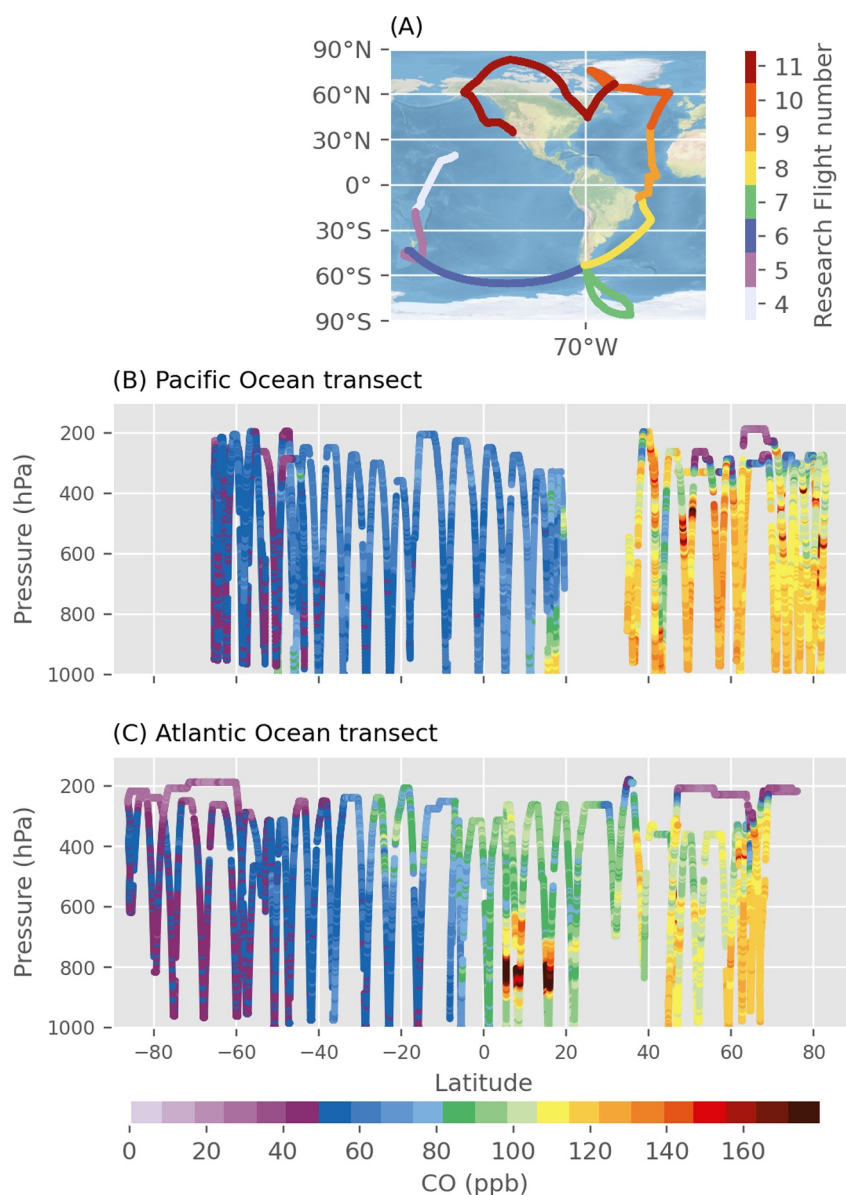


**Figure 1.** ATom-4 campaign flight track location colored by research flight number (a). Altitude versus latitude carbon monoxide atmospheric tomography for (b) Pacific and (c) Atlantic Oceans.

Our ensemble experiments are initialized from a single CAM-chem simulation where the temperature and the winds are nudged to the Modern-Era Retrospective Analysis for Research and Applications version 2 (Gelaro et al., 2017), as in previous studies (Gaubert et al., 2021; Ortega et al., 2023). However, in our ensemble runs that include meteorological DA, the CAM-chem simulations are not nudged to a reanalysis. Sea surface temperatures (SST) are prescribed from a daily analysis of Advanced Very High Resolution Radiometer (AVHRR) observations (Reynolds et al., 2007) on a  $0.25^\circ \times 0.25^\circ$  spatial grid and on a daily timescale. The Community Land Model version 5 (CLM5) is online and coupled to the atmosphere at every physical time step of 30 min. CLM5 is used to calculate the aerosols and gases dry deposition and to drive the Model of Emissions of Gases and Aerosols from Nature, MEGAN v2.1 (Guenther et al., 2012). We are using the specified phenology configuration that prescribes leaf area index. Anthropogenic emissions are provided by the CAMS-GLOB-ANT\_v5.3 inventory, described in detail in Soulie et al. (2024). The Fire INventory from NCAR (Wiedinmyer et al., 2023) version 2.5 (FINNv2.5) estimates daily biomass burning emissions from both the Moderate Resolution Imaging Spectroradiometer (MODIS) and the Visible/Infrared Imager Radiometer Suite (VIIRS). Methane and other greenhouse gases are prescribed at the surface.

### 3.2. Ensemble Adjustment Kalman Filter (EAKF)

The analysis update is estimated by the Ensemble Adjustment Kalman Filter (EAKF) (Anderson, 2001), as implemented in the Data Assimilation Research Testbed (DART), an open-source software for ensemble DA (Anderson et al., 2009). The DA setup used here has been described in detail in Gaubert et al. (2023). It is derived from the CAM + DART reanalysis (Raeder et al., 2021) and includes the MOPITT CO profile assimilation with emission updates (Gaubert et al., 2020).

First a 30-members ensemble of CAM-Chem 6-hourly forecasts is run in parallel. As in previous studies the emissions are perturbed using the pseudo-random fields derived from a two-dimensional Gaussian distribution (Evensen, 2003; Gaubert et al., 2014). This perturbation method compares well with other perturbation strategies (Deng et al., 2022). The same fields are applied to all the species prescribed by the CAMS-GLOB-ANT\_v5.3 anthropogenic inventory with a relative error standard deviation  $\sigma$  of 30% and fixed horizontal decorrelation length  $l$  of 500 km. Another set of fields is applied to all the species emitted by the fire surface emission fluxes with a  $\sigma$  of 20% and  $l$  of 300 km.

The computed ensemble prior provides the meteorological state vector consisting of specific humidity, cloud liquid water, cloud ice, surface pressure, wind components and temperature, as well as the chemical state vector, CO, and surface emissions  $CO_{emi-ant}$  and  $CO_{emi-fire}$ . Let the vector  $z_i^p$ ,  $i = 1, \dots, N$ , represent the prior model state vector for the  $i$ th ensemble forecast valid at a time when observations are assimilated for an  $N$ -member ensemble. DART implements the EAKF using the two-step algorithm described in (Anderson, 2003). The assimilation algorithm can be described without loss of generality by examining the impact of a single observation,  $y$ , on a single component of the model state vector,  $x$ . The first step is to obtain a prior estimate of the observation for each ensemble member by applying a forward operator to the state vector:

$$y_i^p = h(z_i^p), i = 1, \dots, N \quad (1)$$

A normal distribution is fit to the prior ensemble of  $y$ . The observation likelihood is also represented by a normal with a mean equal to the observed value and a specified observation error variance. A continuous normal posterior distribution for  $y$  is computed using Bayes rule to multiply the prior distribution and the likelihood and an analysis (posterior) ensemble,  $y_i^a$ , is computed by conserving the quantiles from the prior ensemble relative to the prior distribution (Anderson, 2022). Increments for the observation are defined as:

$$\Delta y_i = y_i^a - y_i^p \quad (2)$$

In the second step, ensemble increments for each state variable are computed independently in parallel. The increments for state variable  $x$  are computed using the prior ensemble covariance between  $x$  and  $y$  ( $\sigma_{x,y}$ ) and the observation error variance  $\sigma_{y,y}$ :

$$\Delta x_i = \alpha \frac{\sigma_{x,y}}{\sigma_{y,y}} \Delta y_i \quad (3)$$

$\alpha$  is the localization parameter (Anderson, 2012) used to limit the spatial impact of the observations given the sampling errors caused by the small ensemble size. Here we use a half-width 0.1 radians or  $\sim 600$  km for the Gaspari–Cohn localization function (Gaspari & Cohn, 1999) and around 1,200 m in the vertical.

We also estimate emission fluxes using the state augmentation approach. By augmenting the state vector  $z$  with these emission fluxes, we can use (Equation 3) to regress the observation space increments  $\Delta y_i$  onto the unobserved variables, here  $CO_{emi-ant}$  and  $CO_{emi-fire}$ , when assimilating MOPITT CO observations. As in Gaubert et al. (2020), the relative emission increments are used to update the ensemble of emission input files:

$$E_i^a = E_i^p \left( 1 + w \frac{\Delta CO_{emi,i}}{CO_{emi,i}} \right) \quad (4)$$

The weight  $w$  is a function ( $a \exp(-t/(\tau))$ ) used to propagate the increments forward in time with decreasing impacts and set to zero at  $2\tau$ . The EAKF tends to underestimate the uncertainty associated with the prior

distribution due to model error, limited ensemble size, and approximations in the assimilation algorithm. Some of this lost variability is restored using an inflation algorithm applied to the prior. A spatially and temporally varying inflation factor  $\lambda_x$  is applied to each state-space variable (Anderson, 2009) to modify the ensemble spread without affecting the ensemble mean of forecasts  $\bar{x}_i^p$ :

$$x_i^p = \sqrt{\lambda_i} (x_i^p - \bar{x}_i^p) + \bar{x}_i^p \quad (5)$$

The spatially and temporally varying covariance inflation factor  $\lambda_x$  is itself optimized using the enhanced algorithm introduced in Gharamti (2018). The settings for this algorithm include inflation lower and upper bounds of 0 and 25, an inflation standard deviation lower bound of 0.6, and an inflation damping of 0.9. An important parameter is the control of the maximum increase of the inflation standard deviation during one analysis step, it has been set to 1.05.

We note that Ensemble Kalman Filters, like the EAKF, provide optimal solutions if the observation likelihood is Gaussian, the prediction model is linear and if the observation operator is a linear function of the state vector. However, good performance has been achieved with usually slightly nonlinear and non-Gaussian prediction models such as in chemistry applications (e.g., Gaubert et al., 2016).

### 3.3. Quantile-Conserving Ensemble Filter Framework (QCEFF)

The QCEFF generalizes both steps of the EAKF assimilation algorithm. In the first step (Anderson, 2022), computing the increment for the observed variable, an arbitrary distribution can be fit to the prior ensemble of  $y$  that is obtained by applying the forward operator. An arbitrary distribution can also be used for the observation likelihood. Bayes rule is still used to compute the posterior continuous distribution by taking the product of the prior and the likelihood. The posterior ensemble is again obtained by conserving the quantile of the ensemble members. The distribution used here for the prior is the BNRH distribution presented in Appendix C of Anderson (2023) and generalized to allow mixed distributions that have both discrete and continuous probabilities (Anderson et al., 2024). An  $N$ -member ensemble sample of a scalar partitions the real number line into  $N+1$  intervals. The BNRH distribution places  $\frac{1}{N+1}$  of the probability into each region. For interior regions, the probability is uniformly distributed between adjacent ensemble members. If the quantity is bounded, the probability between the outermost ensemble member and the bound is also uniformly distributed. The probability on unbounded tails is represented by an appropriately weighted normal distribution tail. Lower bounds of zero are used for all tracer variables and sources. The likelihood is a truncated normal (Anderson, 2022) for all bounded state variables ( $\text{CO}$ ,  $\text{CO}_{emi-ant}$  and  $\text{CO}_{emi-fire}$ ) and a normal for all other variables.

The QCEFF also generalizes the second step of the EAKF, computing increments for a state variable  $x$  given increments for an observed variable  $y$ , by allowing the regression to be performed in an appropriately transformed space. The  $x$  and  $y$  ensembles are transformed independently for each regression. The transformation is applied using cumulative distribution functions (CDFs)  $F_x^p$  and  $F_y^p$  for all the prior ensemble members for  $x$  and the prior and analysis ensemble members for  $y$ , that is,

$$\tilde{x}_n^p = \Phi^{-1} [F_x^p(x_n^p)] \quad (6)$$

$$\tilde{y}_n^p = \Phi^{-1} [F_y^p(y_n^p)] \quad (7)$$

$$\tilde{x}_n^a = \Phi^{-1} [F_x^a(x_n^a)] \quad (8)$$

where  $\Phi$  is the CDF of a standard normal and  $\Phi^{-1}$  is the probit function or the inverse of the CDF of a standard normal. Again, the BNRH (with a lower bound of 0 for tracers and sources) is the distribution type used to get the CDFs for both the state and observation ensembles.

### 3.4. Assimilation Experiments

We focus on May 2018 because the ATom-4 aircraft observations were available. The month of May is usually characterized by fires, sometimes for agriculture, in the tropics of the northern hemisphere (Duncan et al., 2003).

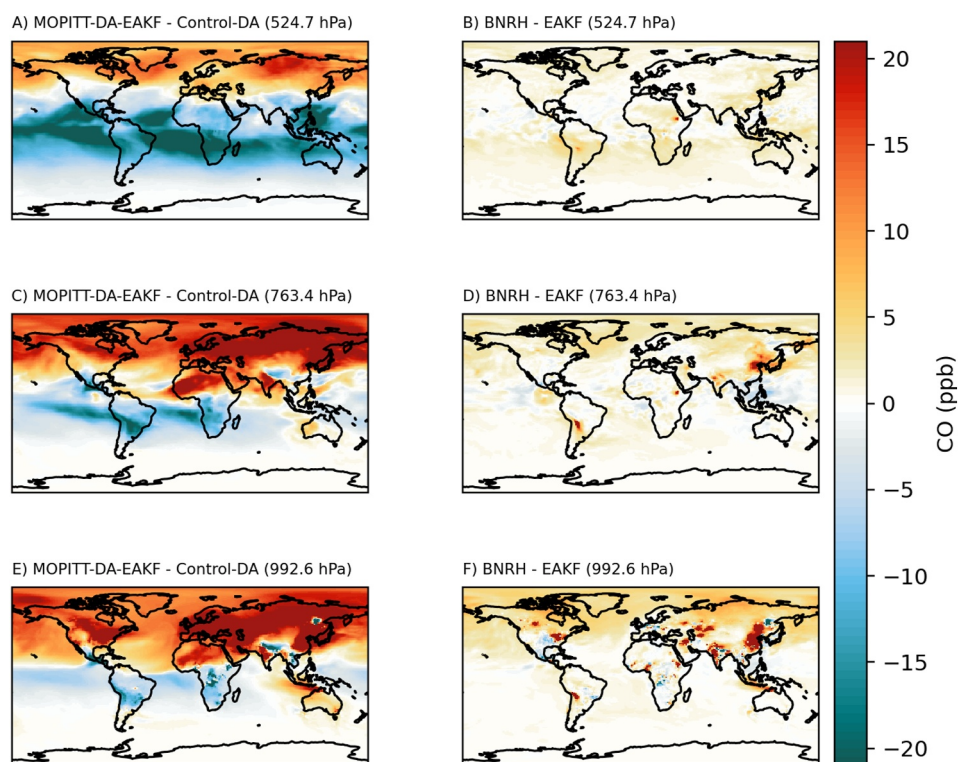


**Figure 2.** Monthly average differences (May 2018) in carbon monoxide (ppb) between MOPITT-DA-EAKF and the Control-DA (left column) and between the MOPITT-DA-BNRH and the MOPITT-DA-EAKF for 3 different altitude levels (~500 hPa, ~700 hPa and for the surface layer).

We carried out 3 assimilation experiments to show the relative impact of the two ensemble filters (EAKF and QCEFF). The ensemble spinup starts on 11 April 2018 with perturbed nudging parameters to generate a dynamical ensemble, and with perturbed emissions. In this case the ensemble is nudged to the CAM6+DART reanalysis (Raeder et al., 2021). The Control-DA (no CO assimilation) is initialized on 17 April 2018 with assimilation of meteorological observations every 6 hr until 1 June 2018. The 2 MOPITT CO assimilation runs (MOPITT-DA-EAKF and the MOPITT-DA-BNRH) are initialized from the Control-DA on 24 April 2018. The MOPITT-DA-BNRH uses QCEFF with BNRH distribution for the CO state and the CO emissions, the meteorological DA is performed as in the other assimilation experiments with an EAKF. The emission optimization for both MOPITT-DA experiments starts on 1 May 2018. We perform 3 additional CAM-chem simulation with the same emissions, but with the updated MOZART TS1.2 chemistry, a reference simulation (CAM-chem-Ref) with the standard emissions (CAMS-GLOB-ANT\_v5.3/FINNV2.5), and with the two obtained posterior emissions for each MOPITT assimilation (CAM-chem-post-EAKF and CAM-chem-post-BNRH).

## 4. Results: Assessment of CO Assimilation Impacts

### 4.1. Assimilation Impacts

Figure 2 shows the assimilation impacts at 3 different altitude layers (524 hPa, 763 hPa and at the surface). The MOPITT assimilation decreases CO across the tropics but increases CO at high latitudes of the northern hemisphere in the free troposphere and to a lesser extent toward the surface. There are larger increases toward the surface and over the continents of the northern hemisphere. Differences between the MOPITT-DA-EAKF and the MOPITT-DA-BNRH remains small but are getting larger toward the surface. CO concentrations can be increased by up to 20 ppb close to large emissions sources, with the most impact in East-Asia. This is likely due to different emission flux estimates. Next, we will compare the various experiments with observational data sets to evaluate the impacts of such CO changes.



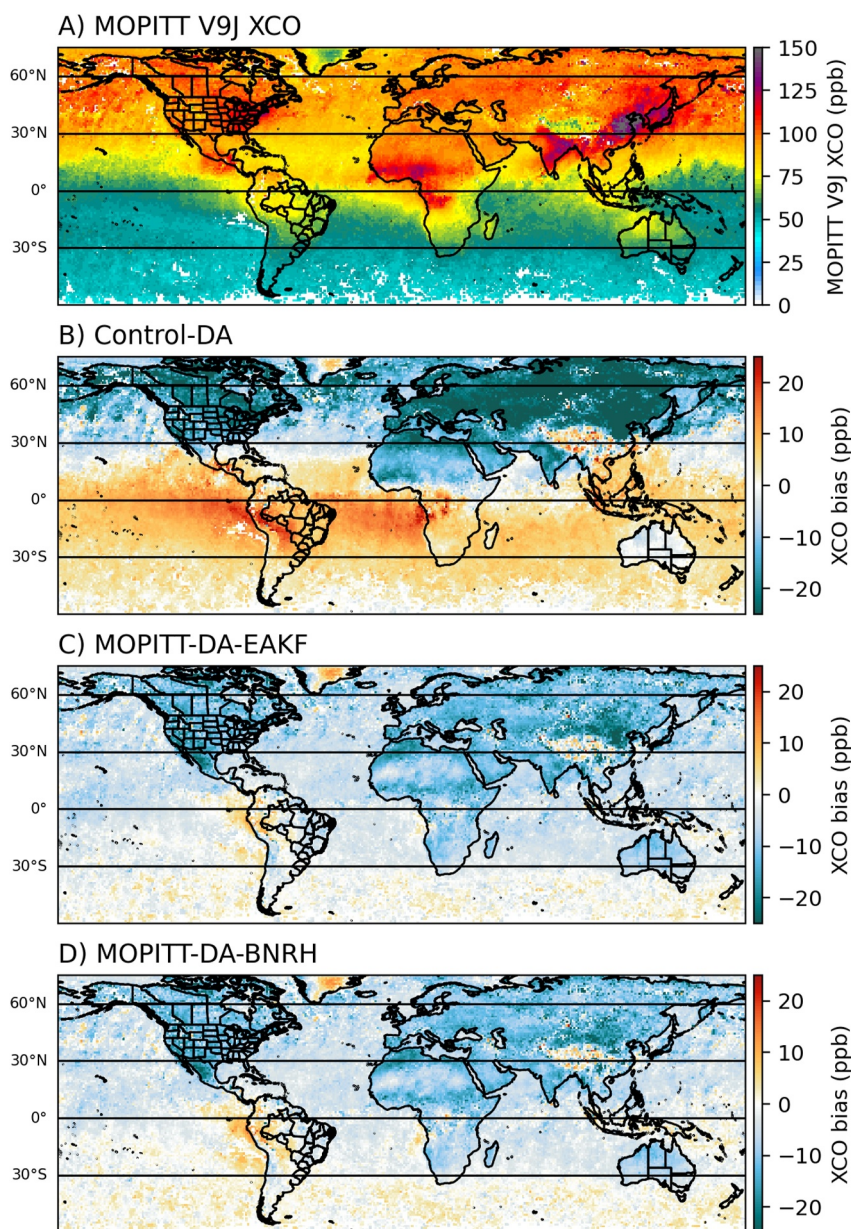


**Figure 3.** MOPITT XCO column-average dry-air mole fraction monthly average (May 2018). Panels b, c, and d show the difference between the model XCO and the MOPITT XCO.

#### 4.2. Comparison With MOPITT XCO

Figure 3a shows the average MOPITT XCO values for the month of May 2018. A common boreal spring feature is the large background values in the northern hemisphere, all greater than 75 ppb. The largest XCO values are found in east and south Asia, western Africa and for a fire in Siberia. One can also notice the fires in central America and in central Africa. Aside from the fire emission plumes, low XCO values ranging from 30 to 60 ppb are found in the southern hemisphere. As in previous studies (Gaubert et al., 2023), the Control-DA overestimates XCO from the tropical fires while underestimating the XCO in the northern hemisphere, by more than 25 ppb (Figure 3). As expected from the result of the MOPITT profile assimilation, the MOPITT-DA-EAKF and the MOPITT-DA-BNRH biases against MOPITT XCO are similar. This suggests good agreement between the two algorithms overall.

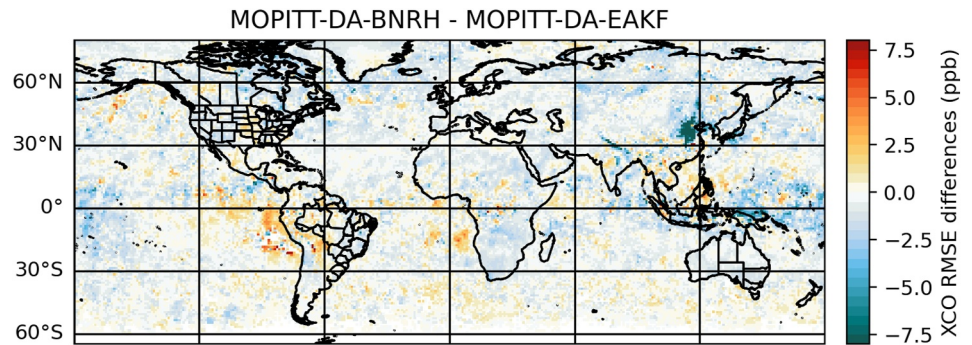


**Figure 4.** Differences in XCO Root mean square errors against MOPITT. It shows the difference between MOPITT-DA-EAKF and MOPITT-DA-BNRH. A negative value indicates an improvement with reduced errors.

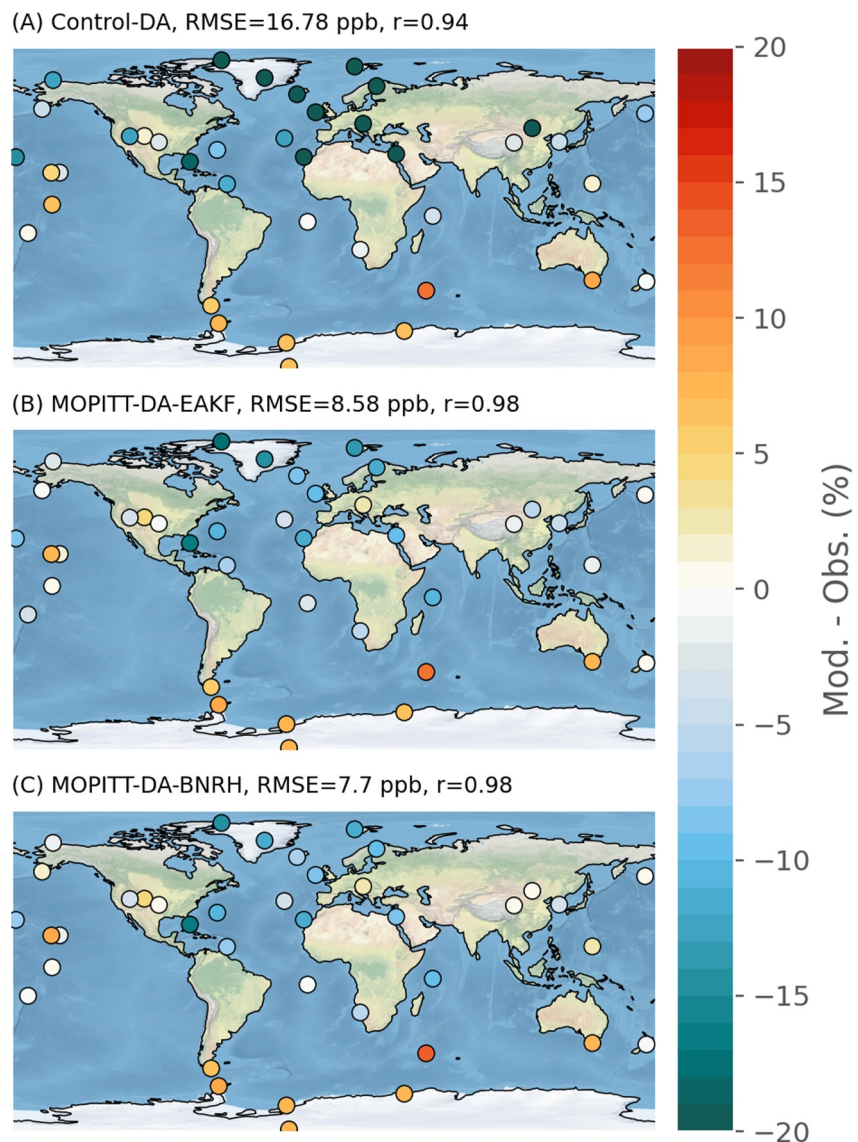


**Figure 5.** Relative bias (%) of the monthly mean (May 2018) carbon monoxide across the global network of surface in-situ flask measurements. Title of each panel also indicates the root mean square errors and the Pearson correlation coefficient  $r$ .

**Table 1**  
Summary Statistics (RMSE) for the Comparison With Independent Set of Observations

Observations	Control-DA	MOPITT-DA-EAKF	MOPITT-DA-BNRH
Surface in-situ (39 stations)	16.8	8.6	7.7
ATom Pacific Ocean ( $N = 14,954$ )	16.05	13.46	13.17
ATom Atlantic Ocean ( $N = 14,605$ )	16.03	15.09	14.83
NDACC wVMR ( $N = 143$ )	21.0	13.0	11.8

Note. The unit of the RMSE is ppb.

Figure 4 displays the impact of BNRH assimilation with respect to the EAKF. It shows the differences in the Root Mean Square Errors (RMSE) against MOPITT XCO, which remains small overall, indicative of similar DA performances. The impact of the assimilation algorithm improves the agreement with MOPITT in East-Asia, around the North China Plain where the CO values were increased at the surface. We will further evaluate the CO with independent data sets in the next sections.

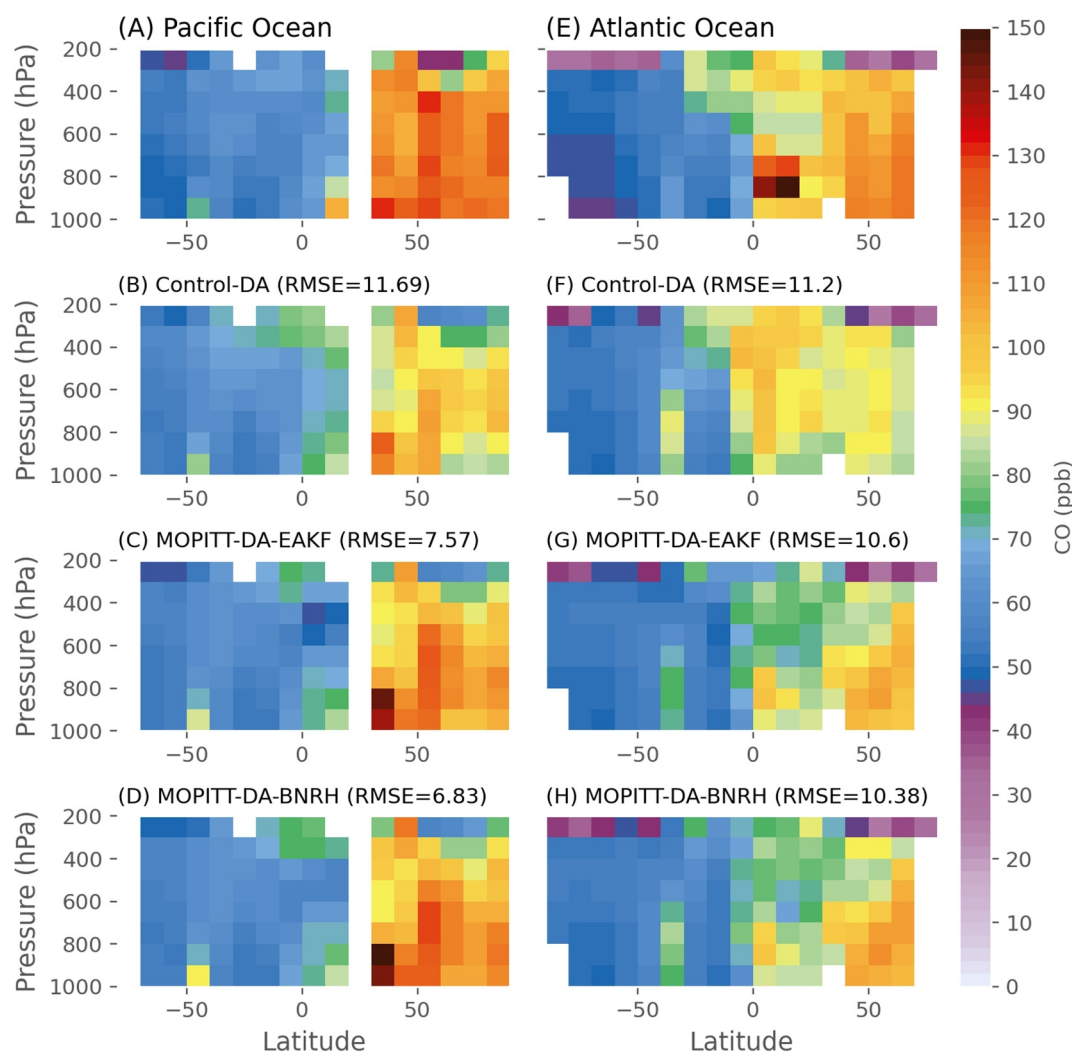


**Figure 6.** ATom-4 carbon monoxide observations (Panels a and b) and assimilation results (other panels) for each ocean basins. The data is bin averaged on a 100 hPa pressure by 10° latitude grid. Global Root Mean Square Errors are indicated for the assimilation results.

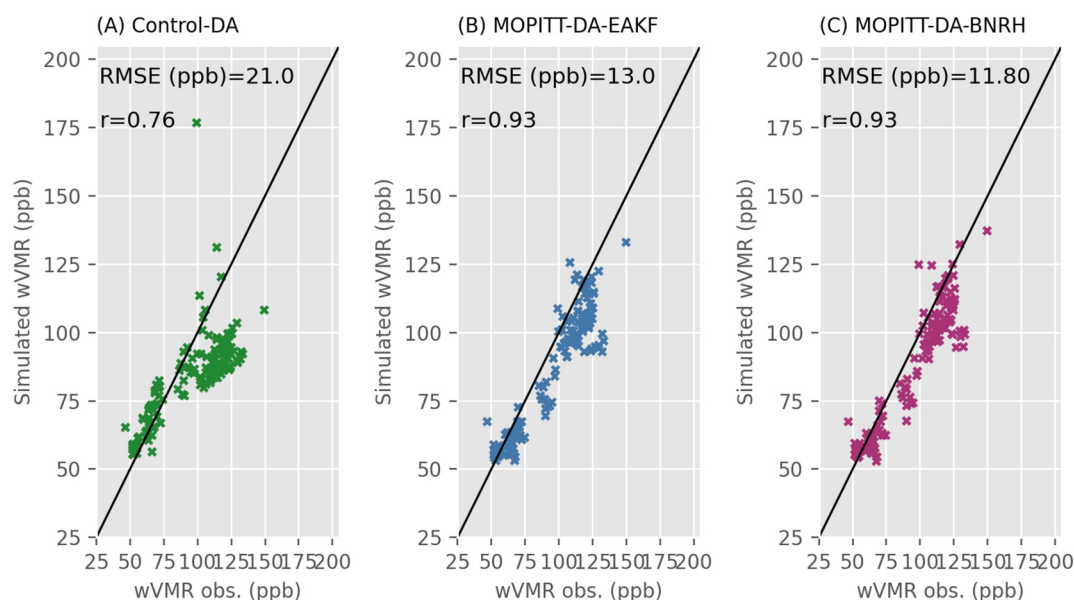


**Figure 7.** Simulated versus observed carbon monoxide wVMR (143 observations across 12 Network for the detection of atmospheric composition change sites) for (a) Control-DA, (b) MOPITT-DA-EAKF, (c) MOPITT-DA-BNRH. The Root Mean Square Errors and the Pearson correlation coefficient are also indicated for each assimilation experiment.

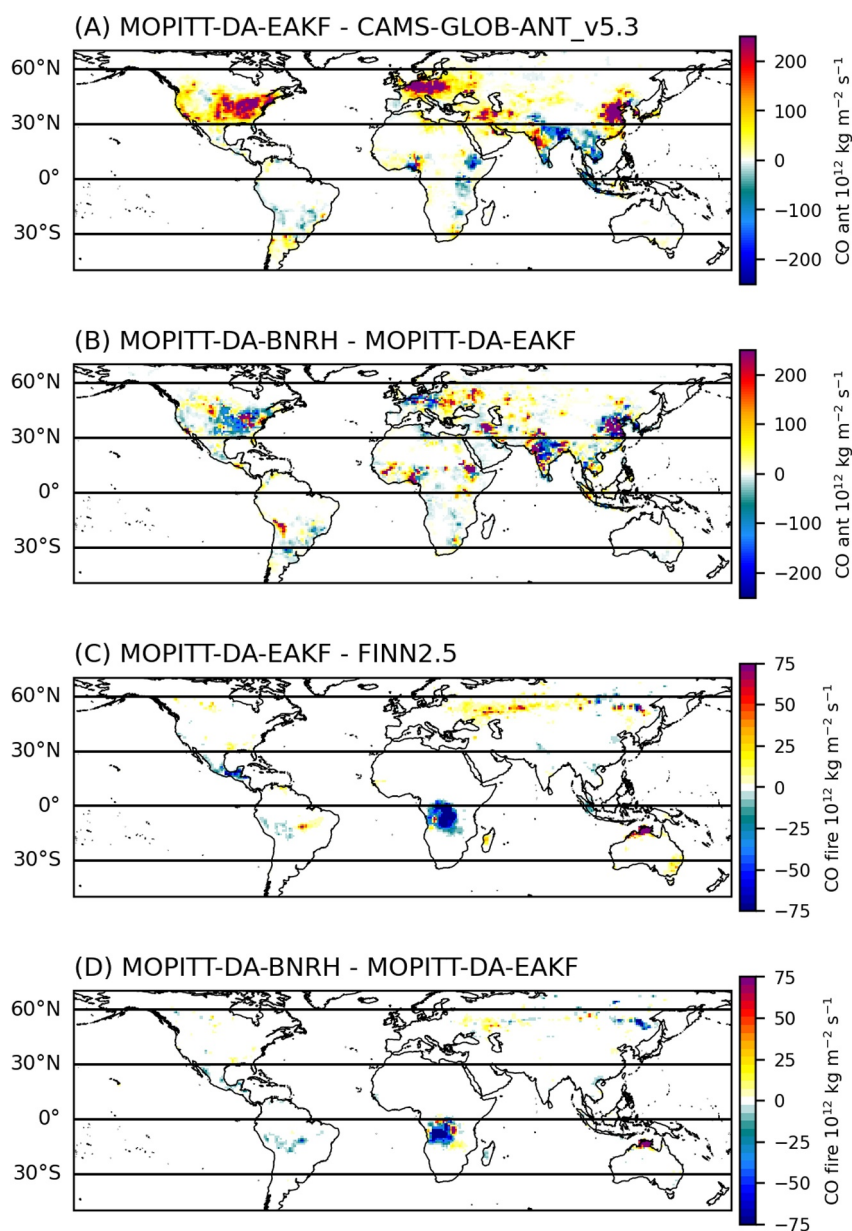
### 4.3. NOAA Global Network of Surface Observations

Figure 5 displays the relative bias at remote surface observation stations for the month of May 2018. The bias pattern is similar to the previous MOPITT XCO comparison, with a CO underestimation of more than 20% in the high latitudes and between 0% and 20% in the rest of the northern hemisphere. Lowest biases are found in the tropics while the high latitudes of the southern hemisphere are overestimated, relative to low CO values. The increase in CO following DA of MOPITT is in good agreement with the surface observations, but does not eliminate the bias over the highest latitudes. This could be simply due to the limited assimilation spinup period since CO assimilation started just a week before the study period, which gave insufficient time to constrain transported CO in this region. The MOPITT-DA-BNRH show a RMSE reduced by around a ppb on average (table 1).

### 4.4. ATom-4

The ATom-4 observations and simulations averaged over 100 hPa pressure by 10° latitude grid are shown in Figure 6. The assimilation of MOPITT improves CO for both ocean basins and reduces the average biases by up to 20 ppb and the global RMSE by around 30%. Overall the differences in the southern hemisphere are much smaller and the assimilation corrects in the right direction, reducing the small overestimation. In the tropics, there are relatively large additional CO enhancements from African and South American fires. Higher observed CO, by up to 30 ppb, is transported in the upper troposphere in the southern hemisphere of the Atlantic Ocean, but not over the Pacific ocean. Despite the challenge of modeling such instantaneous cross section observations, the Control-Run simulation reproduces the shape of the profile with a CO maximum at 300 hPa over the Atlantic Ocean. The MOPITT DA reduces CO in those regions leading to a reduced CO outflow in the upper troposphere for both oceans.

ATom sampled fire plumes at lower altitudes, mostly in the free troposphere in the northern hemisphere. The outflow from Africa sampled in the Northern hemisphere Atlantic is confine to a smaller vertical and horizontal extent than the Control-Run suggests. The MOPITT assimilation reduces CO in the upper troposphere, effectively reducing the bias while not completely capturing the strength of the gradients. The CO tagged tracers from fire source, suggest a large contribution from Asian fires, mainly from Russia. There are small differences between the BNRH and the EAKF algorithms overall, but with the BNRH being consistently better (Table 1).



**Figure 8.** Differences between the posterior and prior emissions flux for May 2018. The top panels (a, b) show the anthropogenic and the bottom panel the fire sources of carbon monoxide.

#### 4.5. Evaluation With NDACC

Figure 7 shows the evaluation of the simulated CO columns (wVMR). As for previous observation data sets, the MOPITT assimilation improves CO by reducing the underestimation in the southern hemisphere, where column observations are in the 50–75 ppb range, and increasing CO in the northern hemisphere. Some of the higher CO observations in the northern hemisphere are underestimated which causes the RMSE to remain higher than 10 ppb. This might be due to the short assimilation period compared to the CO lifetime during the boreal spring and would probably be mitigated more with a longer run. The MOPITT-DA-BNRH RMSE is 11.8 ppb while the MOPITT-DA-EAKF is 13 ppb (Table 1).

#### 4.6. Posterior Emissions

Figure 8 shows the emission increments for the MOPITT-DA-EAKF and the MOPITT-DA-BNRH experiments. The assimilations indicate that CAMS-GLOB-ANT\_v5.3 underestimates anthropogenic CO emissions in China,

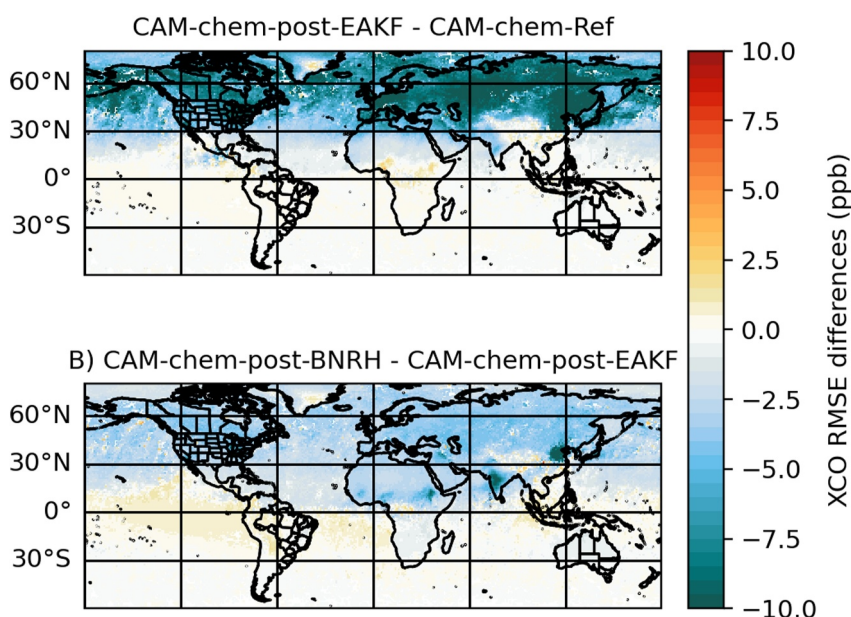


**Figure 9.** Differences in XCO root mean square errors against MOPITT. Panel (a) shows the difference between CAM-chem-REF and CAM-chem-post-EAKF and panel (b) show the difference between CAM-chem-post-BNRH and CAM-chem-post-EAKF. A negative value indicates an improvement with reduced errors.

central Europe, the eastern USA, and the northern portion of the middle east and the Rio de la Plata region. Lower CO emissions are found in Nigeria, Eastern Africa, India, southeast Asia and the state of São Paulo in Brazil. The FINN2.5 are overestimated in the tropics, especially central Africa as well as central America and Indonesia. Positive increments are found in most of Russia and Australia. Differences between the assimilation algorithm revealed different spatial patterns. The MOPITT-DA-BNRH seems to provide increments that are not as smoothed spatially, with larger gradients. At this spatial resolution, there might be wrong attribution of fire related CO enhancements to anthropogenic sources, in particular in regions where both sources are close to each others.

We performed additional CAM-chem simulations with the posterior emissions and evaluate the results against MOPITT XCO (Figure 9). The impact of the simulation using the MOPITT-DA-EAKF is large in the northern hemisphere with a reduction in RMSE larger than 10 ppb over the continent and over the oceanic outflow. The impact is not as important across the tropics and in the southern hemisphere. The simulation using emissions resulting from the MOPITT-DA-BNRH experiment shows lower errors than the simulation using the MOPITT-DA-EAKF posterior emissions across the northern hemisphere and achieve the most improvement in China and India with an additional 10 ppb reduction in RMSE. Since the FINN2.5 over the Congo basin are not reduced as much in the MOPITT-DA-BNRH than for the MOPITT-DA-EAKF estimate, the overestimation persist in the tropics of the southern hemisphere. As discussed in earlier studies (Gaubert et al., 2023), errors in the tropics following chemistry and transport representation are different than for the northern hemisphere and needs to be studied further in future work.

## 5. Conclusions

We present the first large scale geophysical application of the QCEFF or QCEFF. For our chemistry application, where both atmospheric mixing ratio and emission fluxes are positive quantities, we employed a BNRH nonparametric distribution, enforcing the distribution to be satisfy this requirement. This paper presents a comparison of the BNRH and the EAKF algorithm for MOPITT assimilation for 40 days. Overall the differences remain fairly small, suggesting that the EAKF assumption works in most cases.

Our assessment showed that the BNRH algorithm improves CO with regards to 3 different independent data sets, the surface in-situ observations, vertical profiles from NASA ATom-4 and from NDACC ground-based XCO observations. The impact on derived posterior emissions are much larger than for the state assimilation, where the magnitude of the increments is comparable to the MOPITT assimilation. Emission increments can even have a

different sign. CAM-chem simulations with the prior, EAKF- and BNRH-based anthropogenic and fire CO emissions showed an improved fit to MOPITT when the BNRH emissions are used. We consider the BNRH to provide more appropriate results, by providing a distribution that respects the boundaries of the emission distributions. Further improvements can be achieved by assimilating more observational data sets such as Cross-track Infrared Sounder (CrIS), IASI and TROPOMI, and by running at higher spatial and temporal resolution, which will be the basis of future work.

### Data Availability Statement

The MOPITT Version 9 data set is available from NASA through the Earthdata portal (<https://earthdata.nasa.gov/>). CESM2.2 is a publicly released version of the Community Earth System Model that is available at (<https://www.cesm.ucar.edu/>, last access: 15 March 2023). The Data Assimilation Research Testbed is open-source software (version Manhattan; Boulder, Colorado: UCAR/NCAR/CISL/DAReS, <https://doi.org/10.5065/D6WQ0202>); code and documentation are available at (<https://dart.ucar.edu/>, last access: 20 November 2023). Surface in-situ CO flask observations (Pétron et al., 2019) were obtained from the obspack\_co\_1\_GLOBALVIEWplus\_v2.0\_2021-12-08 (Schuldt et al., 2021). The ATom data set is available on the Oak Ridge National Laboratory Distributed Active Archive Center (McKain & Sweeney, 2021; Wofsy et al., 2021).

### References

Anderson, J. L. (2001). An ensemble adjustment kalman filter for data assimilation. *Monthly Weather Review*, 129(12), 2884–2903. [https://doi.org/10.1175/1520-0493\(2001\)129<2884:aeakff>2.0.co;2](https://doi.org/10.1175/1520-0493(2001)129<2884:aeakff>2.0.co;2)

Anderson, J. L. (2003). A local least squares framework for ensemble filtering. *Monthly Weather Review*, 131(4), 634–642. [https://doi.org/10.1175/1520-0493\(2003\)131<0634:allsff>2.0.co;2](https://doi.org/10.1175/1520-0493(2003)131<0634:allsff>2.0.co;2)

Anderson, J. L. (2009). Spatially and temporally varying adaptive covariance inflation for ensemble filters. *Tellus A: Dynamic Meteorology and Oceanography*, 61(1), 72–83. <https://doi.org/10.3402/tellusa.v61i1.15524>

Anderson, J. L. (2010). A non-Gaussian ensemble filter update for data assimilation. *Monthly Weather Review*, 138(11), 4186–4198. <https://doi.org/10.1175/2010mwr3253.1>

Anderson, J. L. (2012). Localization and sampling error correction in ensemble kalman filter data assimilation. *Monthly Weather Review*, 140(7), 2359–2371. <https://doi.org/10.1175/mwr-d-11-00013.1>

Anderson, J. L. (2020). A marginal adjustment rank histogram filter for non-Gaussian ensemble data assimilation. *Monthly Weather Review*, 148(8), 3361–3378. <https://doi.org/10.1175/mwr-d-19-0307.1>

Anderson, J. L. (2022). A quantile-conserving ensemble filter framework. Part I: Updating an observed variable. *Monthly Weather Review*, 150(5), 1061–1074. <https://doi.org/10.1175/mwr-d-21-0229.1>

Anderson, J. L. (2023). A quantile-conserving ensemble filter framework. Part II: Regression of observation increments in a probit and probability integral transformed space. *Monthly Weather Review*, 151(10), 2759–2777. <https://doi.org/10.1175/mwr-d-23-0065.1>

Anderson, J. L., Hoar, T., Raeder, K., Liu, H., Collins, N., Torn, R., & Avellano, A. (2009). The data assimilation research testbed: A community facility. *Bulletin of the American Meteorological Society*, 90(9), 1283–1296. <https://doi.org/10.1175/2009bams2618.1>

Anderson, J. L., Riedel, C., Wieringa, M., Ishraque, F., Smith, M., & Kershaw, H. (2024). A quantile-conserving ensemble filter framework. Part III: Data assimilation for mixed distributions with application to a low-order tracer advection model. *Monthly Weather Review*. <https://doi.org/10.1175/mwr-d-23-0255.1>

Bertagni, M. B., Pacala, S. W., Paulot, F., & Porporato, A. (2022). Risk of the hydrogen economy for atmospheric methane. *Nature Communications*, 13(1), 7706. <https://doi.org/10.1038/s41467-022-35419-7>

Bouarar, I., Gaubert, B., Brasseur, G. P., Steinbrecht, W., Doumbia, T., Tilmes, S., et al. (2021). Ozone anomalies in the free troposphere during the COVID-19 pandemic. *Geophysical Research Letters*, 48(16). <https://doi.org/10.1029/2021gl094204>

Bourgeois, I., Peischl, J., Neuman, J. A., Brown, S. S., Thompson, C. R., Aikin, K. C., et al. (2021). Large contribution of biomass burning emissions to ozone throughout the global remote troposphere. *Proceedings of the National Academy of Sciences*, 118(52), e2109628118. <https://doi.org/10.1073/pnas.2109628118>

Brasseur, G. P., & Kumar, R. (2021). Chemical weather and chemical climate. *AGU Advances*, 2(2). <https://doi.org/10.1029/2021av000399>

Buchholz, R. R., Park, M., Worden, H. M., Tang, W., Edwards, D. P., Gaubert, B., et al. (2022). New seasonal pattern of pollution emerges from changing North American wildfires. *Nature Communications*, 13(1), 2043. <https://doi.org/10.1038/s41467-022-29623-8>

Buchholz, R. R., Worden, H. M., Park, M., Francis, G., Deeter, M. N., Edwards, D. P., et al. (2021). Air pollution trends measured from terra: CO and AOD over industrial fire-prone and background regions. *Remote Sensing of Environment*, 256, 112275. <https://doi.org/10.1016/j.rse.2020.112275>

Butler, T., Lupascu, A., Coates, J., & Zhu, S. (2018). Toast 1.0: Tropospheric ozone attribution of sources with tagging for CESM 1.2.2. *Geoscientific Model Development*, 11(7), 2825–2840. <https://doi.org/10.5194/gmd-11-2825-2018>

Ceamanos, X., Coopman, Q., George, M., Riedel, J., Parrington, M., & Clerboux, C. (2023). Remote sensing and model analysis of biomass burning smoke transported across the Atlantic during the 2020 Western US wildfire season. *Scientific Reports*, 13(1), 16014. <https://doi.org/10.1038/s41598-023-39312-1>

Cheng, Y., Wang, Y., Zhang, Y., Chen, G., Crawford, J. H., Kleb, M. M., et al. (2017). Large biogenic contribution to boundary layer O<sub>3</sub> -CO regression slope in summer. *Geophysical Research Letters*, 44(13), 7061–7068. <https://doi.org/10.1002/2017gl074405>

Cheng, Y., Wang, Y., Zhang, Y., Crawford, J. H., Diskin, G. S., Weinheimer, A. J., & Fried, A. (2018). Estimator of surface ozone using formaldehyde and carbon monoxide concentrations over the eastern United States in summer. *Journal of Geophysical Research: Atmospheres*, 123(14), 7642–7655. <https://doi.org/10.1029/2018jd028452>

Danabasoglu, G., Lamarque, J.-F., Bacmeister, J., Bailey, D. A., DuVivier, A. K., Edwards, J., et al. (2020). The community Earth system model version 2 (CESM2). *Journal of Advances in Modeling Earth Systems*, 12(2). <https://doi.org/10.1029/2019ms001916>

### Acknowledgments

We would like to acknowledge high-performance computing support from Cheyenne (<https://doi.org/10.5065/D6RX99HX>) provided by NSF NCAR's Computational and Information Systems Laboratory, sponsored by the National Science Foundation. The NSF NCAR MOPITT project is supported by the National Aeronautics and Space Administration (NASA) Earth Observing System (EOS) program. The NDACC effort at NSF NCAR is supported under contract by NASA. This material is based upon work supported by the NSF National Center for Atmospheric Research, which is a major facility sponsored by the National Science Foundation under Cooperative Agreement No. 1852977. This study was supported by NOAA's Climate Program Office's Atmospheric Chemistry, Carbon Cycle, and Climate program, Grant #NA18OAR4310283.

- Deeter, M. N., Edwards, D. P., Francis, G. L., Gille, J. C., Mao, D., Martínez-Alonso, S., et al. (2019). Radiance-based retrieval bias mitigation for the MOPITT instrument: The version 8 product. *Atmospheric Measurement Techniques*, *12*(8), 4561–4580. <https://doi.org/10.5194/amt-12-4561-2019>
- Deeter, M. N., Francis, G., Gille, J., Mao, D., Martínez-Alonso, S., Worden, H., et al. (2022). The MOPITT version 9 CO product: Sampling enhancements and validation. *Atmospheric Measurement Techniques*, *15*(8), 2325–2344. <https://doi.org/10.5194/amt-15-2325-2022>
- Deeter, M. N., Mao, D., Martínez-Alonso, S., Worden, H. M., Andreae, M. O., & Schlager, H. (2021). Impacts of MOPITT cloud detection revisions on observation frequency and mapping of highly polluted scenes. *Remote Sensing of Environment*, *262*, 112516. <https://doi.org/10.1016/j.rse.2021.112516>
- Deng, S., Shen, Z., Chen, S., & Wang, R. (2022). Comparison of perturbation strategies for the initial ensemble in ocean data assimilation with a fully coupled Earth system model. *Journal of Marine Science and Engineering*, *10*(3), 412. <https://doi.org/10.3390/jmse10030412>
- Duncan, B. N., Martin, R. V., Staudt, A. C., Yevich, R., & Logan, J. A. (2003). Interannual and seasonal variability of biomass burning emissions constrained by satellite observations. *Journal of Geophysical Research*, *108*(D2). <https://doi.org/10.1029/2002jd002378>
- Elguindi, N., Granier, C., Stavrou, T., Darras, S., Bauwens, M., Cao, H., et al. (2020). Intercomparison of magnitudes and trends in anthropogenic surface emissions from bottom-up inventories top-down estimates and emission scenarios. *Earth's Future*, *8*(8). <https://doi.org/10.1029/2020ef001520>
- Emmons, L. K., Schwantes, R. H., Orlando, J. J., Tyndall, G., Kinnison, D., Lamarque, J.-F., et al. (2020). The chemistry mechanism in the community Earth system model version 2 (CESM2). *Journal of Advances in Modeling Earth Systems*, *12*(4). <https://doi.org/10.1029/2019ms001882>
- Evensen, G. (2003). The ensemble kalman filter: Theoretical formulation and practical implementation. *Ocean Dynamics*, *53*(4), 343–367. <https://doi.org/10.1007/s10236-003-0036-9>
- Gaspari, G., & Cohn, S. E. (1999). Construction of correlation functions in two and three dimensions. *Quarterly Journal of the Royal Meteorological Society*, *125*(554), 723–757. <https://doi.org/10.1002/qj.49712555417>
- Gaubert, B., Arellano, A. F., Barré, J., Worden, H. M., Emmons, L. K., Tilmes, S., et al. (2016). Toward a chemical reanalysis in a coupled chemistry-climate model: An evaluation of MOPITT CO assimilation and its impact on tropospheric composition. *Journal of Geophysical Research: Atmospheres*, *121*(12), 7310–7343. <https://doi.org/10.1002/2016jd024863>
- Gaubert, B., Bouarar, I., Doumbia, T., Liu, Y., Stavrou, T., Deroubaix, A., et al. (2021). Global changes in secondary atmospheric pollutants during the 2020 COVID-19 pandemic. *Journal of Geophysical Research: Atmospheres*, *126*(8). <https://doi.org/10.1029/2020jd034213>
- Gaubert, B., Coman, A., Foret, G., Meleux, F., Ung, A., Rouil, L., et al. (2014). Regional scale ozone data assimilation using an ensemble Kalman filter and the CHIMERE chemical transport model. *Geoscientific Model Development*, *7*(1), 283–302. <https://doi.org/10.5194/gmd-7-283-2014>
- Gaubert, B., Edwards, D. P., Anderson, J. L., Arellano, A. F., Barré, J., Buchholz, R. R., et al. (2023). Global scale inversions from MOPITT CO and MODIS AOD. *Remote Sensing*, *15*(19), 4813. <https://doi.org/10.3390/rs15194813>
- Gaubert, B., Emmons, L. K., Raeder, K., Tilmes, S., Miyazaki, K., Arellano Jr., A. F., et al. (2020). Correcting model biases of CO in East Asia: Impact on oxidant distributions during KORUS-AQ. *Atmospheric Chemistry and Physics*, *20*(23), 14617–14647. <https://doi.org/10.5194/acp-20-14617-2020>
- Gaubert, B., Worden, H. M., Arellano, A. F. J., Emmons, L. K., Tilmes, S., Barré, J., et al. (2017). Chemical feedback from decreasing carbon monoxide emissions. *Geophysical Research Letters*, *44*(19), 9985–9995. <https://doi.org/10.1002/2017gl074987>
- Gelaro, R., McCarty, W., Suárez, M. J., Todling, R., Molod, A., Takacs, L., et al. (2017). The Modern-Era Retrospective analysis for research and applications version 2 (MERRA-2). *Journal of Climate*, *30*(14), 5419–5454. <https://doi.org/10.1175/jcli-d-16-0758.1>
- Gharamti, M. E. (2018). Enhanced adaptive inflation algorithm for ensemble filters. *Monthly Weather Review*, *146*(2), 623–640. <https://doi.org/10.1175/mwr-d-17-0187.1>
- Guenther, A. B., Jiang, X., Heald, C. L., Sakulyanontvittaya, T., Duhl, T., Emmons, L. K., & Wang, X. (2012). The model of emissions of gases and aerosols from nature version 2.1 (MEGAN2.1): An extended and updated framework for modeling biogenic emissions. *Geoscientific Model Development*, *5*(6), 1471–1492. <https://doi.org/10.5194/gmd-5-1471-2012>
- Hudman, R. C., Murray, L. T., Jacob, D. J., Millet, D. B., Turquet, S., Wu, S., et al. (2008). Biogenic versus anthropogenic sources of CO in the United States. *Geophysical Research Letters*, *35*(4). <https://doi.org/10.1029/2007gl032393>
- Inness, A., Aben, I., Ades, M., Borsdorff, T., Flemming, J., Jones, L., et al. (2022). Assimilation of S5P/TROPOMI carbon monoxide data with the global CAMS near-real-time system. *Atmospheric Chemistry and Physics*, *22*(21), 14355–14376. <https://doi.org/10.5194/acp-22-14355-2022>
- Inness, A., Ades, M., Agustí-Panareda, A., Barré, J., Benedictow, A., Blechschmidt, A.-M., et al. (2019). The CAMS reanalysis of atmospheric composition. *Atmospheric Chemistry and Physics*, *19*(6), 3515–3556. <https://doi.org/10.5194/acp-19-3515-2019>
- Jaffe, D. A., & Wigder, N. L. (2012). Ozone production from wildfires: A critical review. *Atmospheric Environment*, *51*, 1–10. <https://doi.org/10.1016/j.atmosenv.2011.11.063>
- Jiang, Z., Jones, D. B. A., Worden, H. M., Deeter, M. N., Henze, D. K., Worden, J., et al. (2013). Impact of model errors in convective transport on CO source estimates inferred from MOPITT CO retrievals. *Journal of Geophysical Research: Atmospheres*, *118*(4), 2073–2083. <https://doi.org/10.1002/jgrd.50216>
- Jiang, Z., Jones, D. B. A., Worden, H. M., & Henze, D. K. (2015). Sensitivity of top-down CO source estimates to the modeled vertical structure in atmospheric CO. *Atmospheric Chemistry and Physics*, *15*(3), 1521–1537. <https://doi.org/10.5194/acp-15-1521-2015>
- Juncosa Calahorrano, J. F., Payne, V. H., Kulawik, S., Ford, B., Flocke, F., Campos, T., & Fischer, E. V. (2021). Evolution of acyl peroxy nitrates (PANs) in wildfire smoke plumes detected by the cross-track infrared sounder (CrIS) over the western U.S. During summer 2018. *Geophysical Research Letters*, *48*(23). <https://doi.org/10.1029/2021gl093405>
- Kopacz, M., Jacob, D. J., Fisher, J. A., Logan, J. A., Zhang, L., Megretskaya, I. A., et al. (2010). Global estimates of CO sources with high resolution by adjoint inversion of multiple satellite datasets (MOPITT AIRS SCIAMACHY TES). *Atmospheric Chemistry and Physics*, *10*(3), 855–876. <https://doi.org/10.5194/acp-10-855-2010>
- Lama, S., Houweling, S., Boersma, K. F., Aben, I., van der Gon, H. A. C. D., & Krol, M. C. (2022). Estimation of OH in urban plumes using TROPOMI-inferred NO<sub>2</sub>/CO. *Atmospheric Chemistry and Physics*, *22*(24), 16053–16071. <https://doi.org/10.5194/acp-22-16053-2022>
- Lin, M., Horowitz, L. W., Payton, R., Fiore, A. M., & Tonnesen, G. (2017). US surface ozone trends and extremes from 1980 to 2014: Quantifying the roles of rising Asian emissions domestic controls wildfires and climate. *Atmospheric Chemistry and Physics*, *17*(4), 2943–2970. <https://doi.org/10.5194/acp-17-2943-2017>
- Liu, J., Bowman, K. W., Schimel, D. S., Parazoo, N. C., Jiang, Z., Lee, M., et al. (2017). Contrasting carbon cycle responses of the tropical continents to the 2015–2016 El Niño. *Science*, *358*(6360), eaam5690. <https://doi.org/10.1126/science.aam5690>
- Liu, X., Ma, P.-L., Wang, H., Tilmes, S., Singh, B., Easter, R. C., et al. (2016). Description and evaluation of a new four-mode version of the modal aerosol module (MAM4) within version 5.3 of the community atmosphere model. *Geoscientific Model Development*, *9*(2), 505–522. <https://doi.org/10.5194/gmd-9-505-2016>



- McKain, K., & Sweeney, C. (2021). *ATom: CO<sub>2</sub>, CH<sub>4</sub> and CO measurements from picarro 2016-2018*. ORNL Distributed Active Archive Center. <https://doi.org/10.3334/ORNDAAC/1732>
- Miyazaki, K., Eskes, H., Sudo, K., Boersma, K. F., Bowman, K., & Kanaya, Y. (2017). Decadal changes in global surface NO<sub>x</sub> emissions from multi-constituent satellite data assimilation. *Atmospheric Chemistry and Physics*, *17*(2), 807–837. <https://doi.org/10.5194/acp-17-807-2017>
- Müller, J.-F., Stavrou, T., Bauwens, M., George, M., Hurtmans, D., Coheur, P.-F., et al. (2018). Top-down CO emissions based on IASI observations and hemispheric constraints on OH levels. *Geophysical Research Letters*, *45*(3), 1621–1629. <https://doi.org/10.1002/2017gl076697>
- Naus, S., Domingues, L. G., Krol, M., Luijckx, I. T., Gatti, L. V., Miller, J. B., et al. (2022). Sixteen years of MOPITT satellite data strongly constrain Amazon CO fire emissions. *Atmospheric Chemistry and Physics*, *22*(22), 14735–14750. <https://doi.org/10.5194/acp-22-14735-2022>
- Novelli, P. C., Elkins, J. W., & Steele, L. P. (1991). The development and evaluation of a gravimetric reference scale for measurements of atmospheric carbon monoxide. *Journal of Geophysical Research*, *96*(D7), 13109–13121. <https://doi.org/10.1029/91jd01108>
- Novelli, P. C., Masarie, K. A., Lang, P. M., Hall, B. D., Myers, R. C., & Elkins, J. W. (2003). Reanalysis of tropospheric CO trends: Effects of the 1997–1998 wildfires. *Journal of Geophysical Research*, *108*(D15). <https://doi.org/10.1029/2002jd003031>
- Ortega, I., Gaubert, B., Hannigan, J. W., Brasseur, G., Worden, H. M., Blumenstock, T., et al. (2023). Anomalies of O<sub>3</sub>, CO, C<sub>2</sub>H<sub>2</sub>, H<sub>2</sub>CO and C<sub>2</sub>H<sub>6</sub> detected with multiple ground-based fourier-transform infrared spectrometers and assessed with model simulation in 2020: COVID-19 lockdowns versus natural variability. *Elementa: Science of the Anthropocene*, *11*(1). <https://doi.org/10.1525/elementa.2023.00015>
- Parazoo, N. C., Bowman, K. W., Baier, B. C., Liu, J., Lee, M., Kuai, L., et al. (2021). Covariation of airborne biogenic tracers (CO<sub>2</sub>, COS and CO) supports stronger than expected growing season photosynthetic uptake in the southeastern US. *Global Biogeochemical Cycles*, *35*(10). <https://doi.org/10.1029/2021gb006956>
- Pétron, G., Crotwell, A., Crotwell, M., Dlugokencky, E., Madronich, M., Moglia, E., et al. (2019). *Earth system research laboratory carbon cycle and greenhouse gases group flask-air sample measurements of CO at global and regional background sites, 1967-present*. NOAA ESRL GML CCGG Group. <https://doi.org/10.15138/33BV-S284>
- Peuch, V.-H., Engelen, R., Dee, M. R. D., Flemming, J., Suttie, M., Ades, M., et al. (2022). The Copernicus atmosphere monitoring Service: From research to operations. *Bulletin of the American Meteorological Society*, *103*(12), E2650–E2668. <https://doi.org/10.1175/bams-d-21-0314.1>
- Prather, M. J. (2007). Lifetimes and time scales in atmospheric chemistry. *Philosophical Transactions of the Royal Society A: Mathematical, Physical & Engineering Sciences*, *365*(1856), 1705–1726. <https://doi.org/10.1098/rsta.2007.2040>
- Qu, Z., Henze, D. K., Worden, H. M., Jiang, Z., Gaubert, B., Theys, N., & Wang, W. (2022). Sector-based top-down estimates of NO<sub>x</sub>, SO<sub>2</sub> and CO emissions in East Asia. *Geophysical Research Letters*, *49*(2). <https://doi.org/10.1029/2021gl096009>
- Raeder, K., Hoar, T. J., El-Gharamti, M., Johnson, B. K., Collins, N., Anderson, J. L., et al. (2021). A new CAM6 + DART reanalysis with surface forcing from CAM6 to other CESM models. *Scientific Reports*, *11*(1), 16384. <https://doi.org/10.1038/s41598-021-92927-0>
- Reynolds, R. W., Smith, T. M., Liu, C., Chelton, D. B., Casey, K. S., & Schlax, M. G. (2007). Daily high-resolution-blended analyses for sea surface temperature. *Journal of Climate*, *20*(22), 5473–5496. <https://doi.org/10.1175/2007jcli1824.1>
- Schuldtt, K. N., Aalto, T., Andrews, A., Baier, B., Bergamaschi, P., Biermann, T., et al. (2021). *Multi-laboratory compilation of atmospheric carbon monoxide data for the period 1989-2020; obspack\_co\_1\_GLOBALVIEWplus\_v2.0\_2021-12-08*. NOAA Global Monitoring Laboratory. Retrieved from [https://gml.noaa.gov/ccgg/obspack/data.php?id=obspack\\_co\\_1\\_GLOBALVIEWplus\\_v2.0\\_2021-12-08](https://gml.noaa.gov/ccgg/obspack/data.php?id=obspack_co_1_GLOBALVIEWplus_v2.0_2021-12-08)
- Shindell, D. T., Faluvegi, G., Stevenson, D. S., Krol, M. C., Emmons, L. K., Lamarque, J.-F., et al. (2006). Multimodel simulations of carbon monoxide: Comparison with observations and projected near-future changes. *Journal of Geophysical Research*, *111*(D19). <https://doi.org/10.1029/2006jd007100>
- Silva, S. J., Arellano, A. F., & Worden, H. M. (2013). Toward anthropogenic combustion emission constraints from space-based analysis of urban CO<sub>2</sub>/CO sensitivity. *Geophysical Research Letters*, *40*(18), 4971–4976. <https://doi.org/10.1002/grl.50954>
- Soulie, A., Granier, C., Darras, S., Zilbermann, N., Doumbia, T., Guevara, M., et al. (2024). Global anthropogenic emissions (CAMS-GLOB-ANT) for the Copernicus Atmosphere Monitoring Service simulations of air quality forecasts and reanalyses. *Earth System Science Data*, *16*(5), 2261–2279. <https://doi.org/10.5194/essd-16-2261-2024>
- Staniaszek, Z., Griffiths, P. T., Folberth, G. A., O'Connor, F. M., Abraham, N. L., & Archibald, A. T. (2022). The role of future anthropogenic methane emissions in air quality and climate. *NPJ Climate and Atmospheric Science*, *5*(1), 21. <https://doi.org/10.1038/s41612-022-00247-5>
- Stein, O., Schultz, M. G., Bouarar, I., Clark, H., Huijnen, V., Gaudel, A., et al. (2014). On the wintertime low bias of Northern Hemisphere carbon monoxide found in global model simulations. *Atmospheric Chemistry and Physics*, *14*(17), 9295–9316. <https://doi.org/10.5194/acp-14-9295-2014>
- Tang, W., Arellano, A. F., Gaubert, B., Miyazaki, K., & Worden, H. M. (2019). Satellite data reveal a common combustion emission pathway for major cities in China. *Atmospheric Chemistry and Physics*, *19*(7), 4269–4288. <https://doi.org/10.5194/acp-19-4269-2019>
- Tang, Z., Chen, J., & Jiang, Z. (2022). Discrepancy in assimilated atmospheric CO over East Asia in 2015–2020 by assimilating satellite and surface CO measurements. *Atmospheric Chemistry and Physics*, *22*(11), 7815–7826. <https://doi.org/10.5194/acp-22-7815-2022>
- Thompson, C. R., Wofsy, S. C., Prather, M. J., Newman, P. A., Hanisco, T. F., Ryerson, T. B., et al. (2022). The NASA atmospheric tomography (ATom) mission: Imaging the chemistry of the global atmosphere. *Bulletin of the American Meteorological Society*, *103*(3), E761–E790. <https://doi.org/10.1175/bams-d-20-0315.1>
- Tian, Y., Liu, C., Sun, Y., Borsdorff, T., Landgraf, J., Lu, X., et al. (2022). Satellite observations reveal a large CO<sub>2</sub> emission discrepancy from industrial point sources over China. *Geophysical Research Letters*, *49*(5). <https://doi.org/10.1029/2021gl097312>
- Tilmes, S., Hodzic, A., Emmons, L. K., Mills, M. J., Gettelman, A., Kinnison, D. E., et al. (2019). Climate forcing and trends of organic aerosols in the community Earth system model (CESM2). *Journal of Advances in Modeling Earth Systems*, *11*(12), 4323–4351. <https://doi.org/10.1029/2019ms001827>
- van der Velde, I. R., van der Werf, G. R., Houweling, S., Maasackers, J. D., Borsdorff, T., Landgraf, J., et al. (2021). Vast CO<sub>2</sub> release from Australian fires in 2019–2020 constrained by satellite. *Nature*, *597*(7876), 366–369. <https://doi.org/10.1038/s41586-021-03712-y>
- Wiedinmyer, C., Kimura, Y., McDonald-Buller, E. C., Emmons, L. K., Buchholz, R. R., Tang, W., et al. (2023). The fire inventory from NCAR version 2.5: An updated global fire emissions model for climate and chemistry applications. *Geoscientific Model Development*, *16*(13), 3873–3891. <https://doi.org/10.5194/gmd-16-3873-2023>
- Wilka, C., Solomon, S., Kinnison, D., & Tarasick, D. (2021). An Arctic ozone hole in 2020 if not for the Montreal Protocol. *Atmospheric Chemistry and Physics*, *21*(20), 15771–15781. <https://doi.org/10.5194/acp-21-15771-2021>
- Wofsy, S., Afshar, S., Allen, H., Apel, E., Asher, E., Barletta, B., et al. (2021). *Atom: Merged atmospheric chemistry trace gases and aerosols version 2 [dataset]*. ORNL Distributed Active Archive Center. <https://doi.org/10.3334/ORNDAAC/1925>
- Worden, H. M., Bloom, A. A., Worden, J. R., Jiang, Z., Marais, E. A., Stavrou, T., et al. (2019). New constraints on biogenic emissions using satellite-based estimates of carbon monoxide fluxes. *Atmospheric Chemistry and Physics*, *19*(21), 13569–13579. <https://doi.org/10.5194/acp-19-13569-2019>

- Worden, H. M., Deeter, M. N., Edwards, D. P., Gille, J. C., Drummond, J. R., & Nédélec, P. (2010). Observations of near-surface carbon monoxide from space using MOPITT multispectral retrievals. *Journal of Geophysical Research*, *115*(D18). <https://doi.org/10.1029/2010jd014242>
- Wu, D., Liu, J., Wennberg, P. O., Palmer, P. I., Nelson, R. R., Kiel, M., & Eldering, A. (2022). Towards sector-based attribution using intra-city variations in satellite-based emission ratios between CO<sub>2</sub> and CO. *Atmospheric Chemistry and Physics*, *22*(22), 14547–14570. <https://doi.org/10.5194/acp-22-14547-2022>
- Zhao, Y., Saunio, M., Bousquet, P., Lin, X., Berchet, A., Hegglin, M. I., et al. (2020). On the role of trend and variability in the hydroxyl radical (OH) in the global methane budget. *Atmospheric Chemistry and Physics*, *20*(21), 13011–13022. <https://doi.org/10.5194/acp-20-13011-2020>
- Zheng, B., Chevallier, F., Yin, Y., Ciais, P., Fortems-Cheiney, A., Deeter, M. N., et al. (2019). Global atmospheric carbon monoxide budget 2000–2017 inferred from multi-species atmospheric inversions. *Earth System Science Data*, *11*(3), 1411–1436. <https://doi.org/10.5194/essd-11-1411-2019>
- Zheng, B., Ciais, P., Chevallier, F., Yang, H., Canadell, J. G., Chen, Y., et al. (2023). Record-high CO<sub>2</sub> emissions from boreal fires in 2021. *Science*, *379*(6635), 912–917. <https://doi.org/10.1126/science.ade0805>